Atomic force microscopy investigation of growth process of organic TCNQ aggregates on SiO_2 and mica substrates*

Huan Qing(郇 庆), Hu Hao(胡 昊), Pan Li-Da(潘理达),
Xiao Jiang(肖 江), Du Shi-Xuan(杜世萱), and Gao Hong-Jun(高鸿钧)†

Institute of Physics, Chinese Academy of Sciences, Beijing 100190, *China*

(Received 26 January 2010; revised manuscript received 4 February 2010)

Deposition patterns of tetracyanoquinodimethane (TCNQ) molecules on different surfaces are investigated by atomic force microscopy. A homemade physical vapour deposition system allows the better control of molecule deposition. Taking advantage of this system, we investigate TCNQ thin film growth on both SiO_2 and mica surfaces. It is found that dense island patterns form at a high deposition rate, and a unique seahorse-like pattern forms at a low deposition rate. Growth patterns on different substrates suggest that the fractal pattern formation is dominated by molecule–molecule interaction. Finally, a phenomenal "two-branch" model is proposed to simulate the growth process of the seahorse pattern.

Keywords: tetracyanoquinodimethane, organic molecule deposition, seahorse-like patterns

PACC: 0555, 6116P, 6855

1. Introduction

Organic functional nanostructures on solid surfaces were investigated extensively for fundamental research and practical applications.[1−5] The study of organic thin film growth[6−8] at the molecular level was motivated by the ever greater requirements for developing the next generation of optical, electronic and magnetic devices,[9] as well as for understanding the microcosmic structures,[10] due to the specific characteristics of organic thin films.

Understanding the evolution of surface morphology, such as the formation of compact and fractal patterns[11,12] during organic thin film growth, is a crucial step toward the controlling of the growth of organic nanostructures. Here we report our investigation of fractal patterns of 7, 7′, 8, 8′-tetracyanoquinodimethane (TCNQ) molecules on SiO_2 and mica surfaces. The molecular structure of TCNQ is shown in Fig. 1. TCNQ[13,14] is a good one-electron acceptor, and salts of the resulting radical anion show a wide range of interesting electronic properties like high electrical conductivity[15] and ferromagnetic characteristics.[16] TCNQ can be used as electrode material in novel organic electrolytic capacitors and has potential applications in bistable-threshold or memory switches,[17,18] molecular magnets[19,20] and molecular sensors.[21] Moreover, the unique seahorse-like fractal aggregations[22−30] of TCNQ or its derivatives are pivotal for understanding the growth process of organic thin films in general.

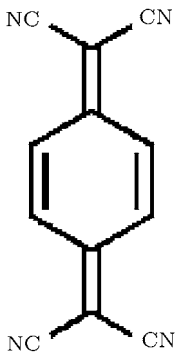


Fig. 1. Chemical structure of 7, 7′, 8, 8′-tetracyanoquinodimethane (TCNQ) molecule.

In most of the earlier work on TCNQ fractal patterns, the scanning electron microscopy (SEM) or transmission electron microscopy (TEM) and amorphous carbon substrates[22−26] were used to study the transmission properties of the material, which in turn reveal the crystalline character and thickness of the

*Project supported by the National Natural Science Foundation of China (Grant No. 10774176), and the National Basic Research Program of China (Grant No. 2006CB806202).

†Corresponding author. E-mail: hjgao@aphy.iphy.ac.cn

© 2010 Chinese Physical Society and IOP Publishing Ltd

thin film. To investigate the growth process of the surface morphology of TCNQ thin film, we use atomic force microscopy (AFM). We use a secondary physical vapour deposition (SPVD) method to deposit TCNQ thin films on SiO_2 and mica surfaces under different conditions. Further characterizations by ambient atomic force microscopy reveal that the seahorse-like fractal patterns can be formed on these two inert substrates and the growth conditions have a great effect on the molecular deposition patterns.

2. Experiments

We develop a secondary physical vapour deposition (SPVD) system for the preparation of samples. Unlike traditional physical vapour deposition methods, SPVD has two deposition steps in a high vacuum environment. The critical component we used here is a hand tailored quartz crucible which has two separate cavities, i.e., the primary cavity, which can be heated directly by a tungsten filament and the secondary cavity, which is open to the primary cavity and can be heated only through heat exchange. In the first step, highly pure (98%) TCNQ molecules preloaded in the primary cavity are deposited onto the wall of the secondary cavity when the filament temperature reaches 360 K. Then, when the filament temperature is increased to 468 K, the TCNQ molecules vapourize from the wall of the secondary cavity and form a film on the substrate.

This SPVD method has several advantages for the deposition of organic materials. 1) The SPVD process is a clean deposition process under high vacuum. 2) The two-step process can purify organic specimens. 3) SPVD has more accurate deposition flux control since the temperature gradients on the wall of the secondary cavity play an important role during deposition. With our SPVD method, an extremely finely tuned deposition flux can be realized. 4) For colourful specimens, the deposition quantity is visible in the secondary cavity of the crucible. So, precise deposition quantity control can be achieved by this method. 5) The cost of this SPVD method is much lower than that of molecular beam epitaxy (MBE).

TCNQ molecules are deposited onto the substrates at room temperature in a high vacuum with a base pressure better than 5×10^{-5} Pa. Then we use AFM to characterize the surface morphology. We use SiO_2 and mica as substrates.

3. Results and discussion

3.1. TCNO deposit patterns

As shown in Fig. 2(a), highly uniform dot patterns in a large area can be obtained at deposition flux (F) as high as 50 nm/min for 4 min. In this case, the density of the molecules on the surface is too high and the diffusion of the molecules is limited; the molecules can diffuse only a very short distance and collide with each other to form high-density islands.[6] At a lower deposition flux, 25 nm/min, the diffusion of the molecules is partially enhanced, and we are able to obtain bug-like patterns as shown in Fig. 2(b). The bug-like patterns can be thought of as the initial modality of the seahorse-like patterns. Further decreasing the deposition flux to 20 nm/min or 9 nm/min leads to a mixture (Fig. 2(c)) of seahorse-like patterns and bug-like patterns, or exclusively seahorse-like patterns (Fig. 2(d)).

According to Figs. 2(a)–2(d), it is obvious that the deposition flux has a great effect on the formation of organic patterns. The unique seahorse-like fractal patterns of TCNQ molecules can be obtained only at low deposition flux, which allows the molecules to relatively freely diffuse.

3.2. TCNQ thin films

Organic electronic and optoelectronic devices require high quality materials in different forms, such as organic quantum dots[31] and organic thin films.[32] By taking advantage of the SPVD method we can control deposition conditions very well and furthermore, control the growth of organic patterns. Figure 3 shows how to grow different TCNQ thin films by adjusting deposition conditions. When the deposition quantity is small, only a few isolated islands form on the surface (Fig. 3(a)), separated by empty zones. At higher deposition quantities, isolated islands will coalesce to form thin films as shown in Figs. 3(b) and 3(c). TCNQ thin films grown at room temperature are not well-proportioned. The initial islands can still be seen in the thin films. This implies that the thin film growth follows the same process as the island growth. By varying the deposition flux, we can control the quality of the thin film. Figures 3(b) and 3(c) show two kinds of TCNQ thin films with almost the same coverage rate on SiO_2 substrate.

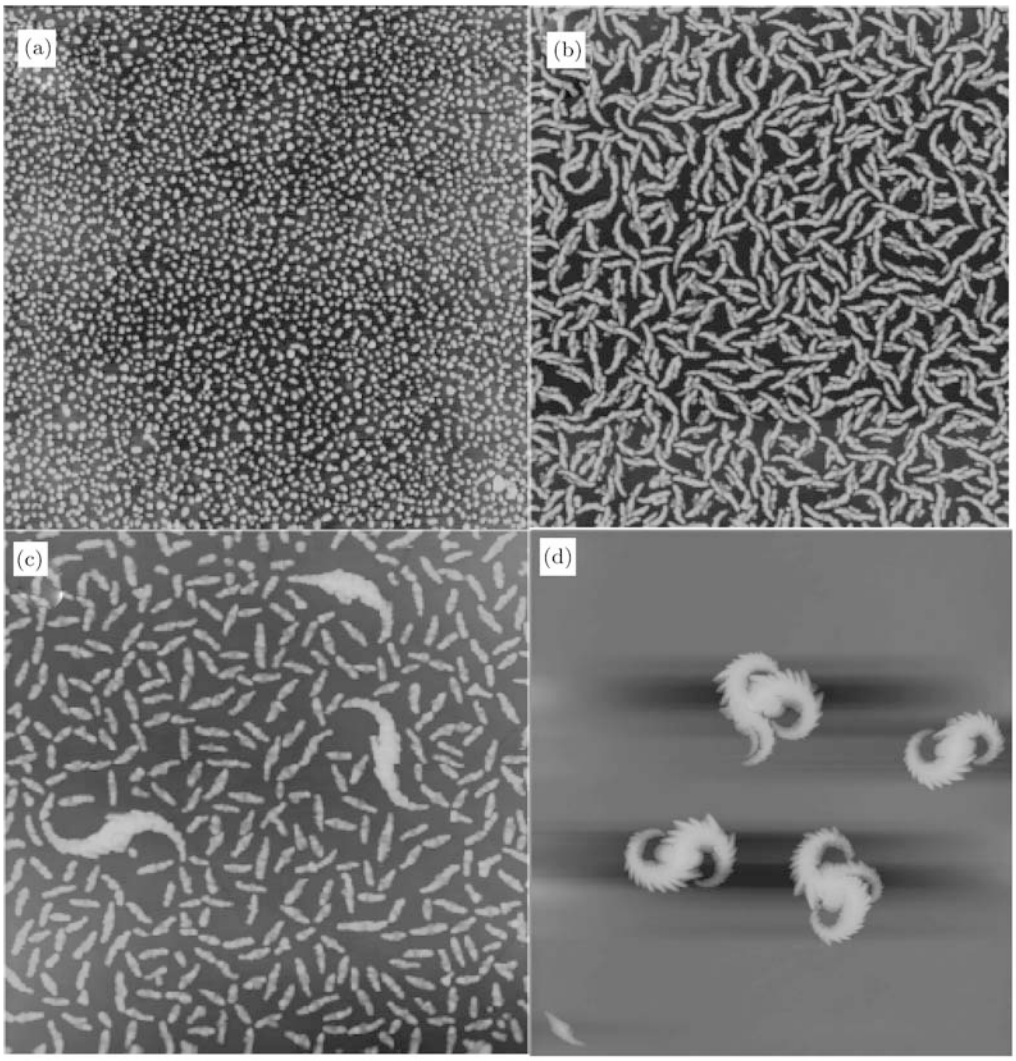


Fig. 2. Deposition patterns of TNCQ on SiO_2 at different values of deposition flux F: (a) 20 μm×20 μm, dot patterns formed at $F = 50$ nm/min; (b) 20 μm×20 μm, bug-like patterns formed at $F = 25$ nm/min; (c) 20 μm×20 μm, mixture of bug-like patterns and seahorse-like patterns formed at $F = 20$ nm/min; (d) 40 μm×40 μm, seahorse-like patterns formed at $F = 9$ nm/min.

It is clear that the two films are formed from very similar islands, but the sizes of islands in the two films are quite different. The thin film in Fig. 3(b) contains smaller preformed islands due to higher deposition flux (22 nm/min). Accordingly, at lower deposition flux a flatter thin film with bigger islands inside is obtained.

3.3. Seahorse-like fractal patterns on different substrates

A deeper understanding of the mechanism behind the formation of the seahorse patterns requires extended experimental data. The previous work on this unique fractal patterns was done mainly on amorphous carbon thin film and characterized by SEM or TEM.[22−26] Here we successfully grew the seahorse-like patterns on both SiO_2 and mica surfaces, then characterized them with an ambient atomic force microscope operating in a contact mode. SiO_2 surface is amorphous and has weak isotropic interactions with the adsorbate.[27,28,33] While mica is a monoclinic crystal, and the surface facet of (001) is a hexagonal lattice.[27,28,34] A comparison of the fractal patterns on different substrates allows us to understand the interplay between molecule–molecule interactions and molecule–surface interactions during the process and address the physics of formation of the seahorse patterns.

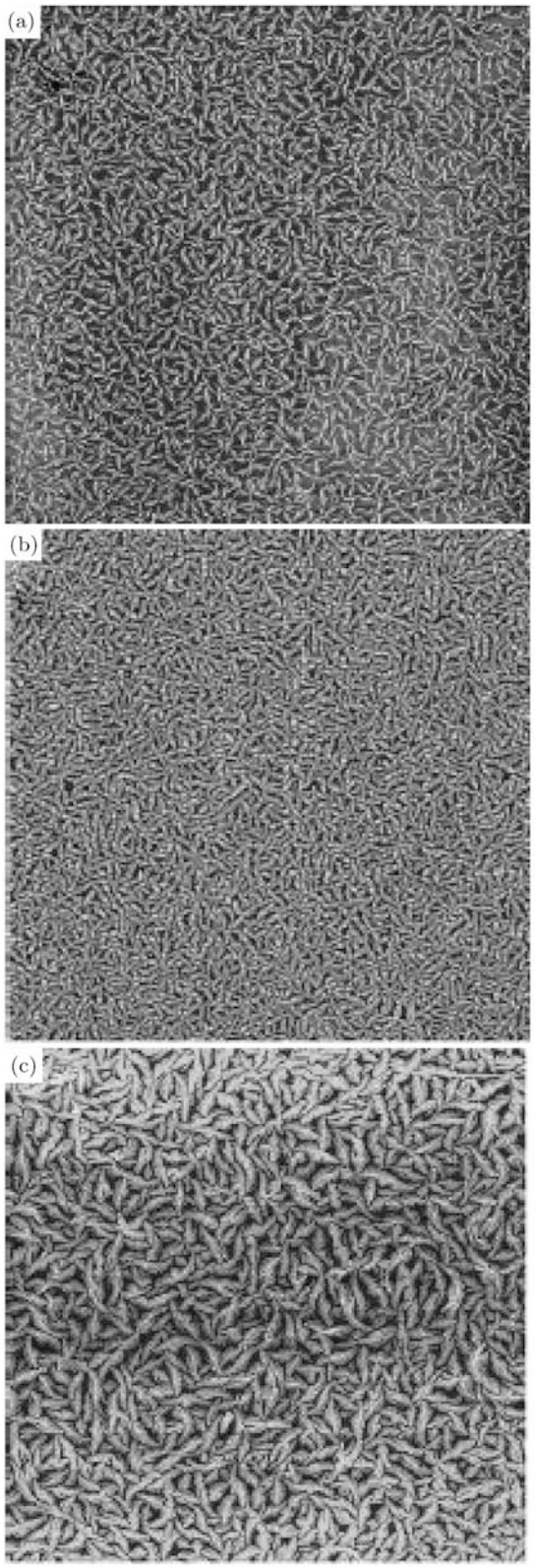


Fig. 3. Deposition process of TCNQ thin film on SiO_2 at different values of deposition flux F: (a) 50 μm×50 μm F = 24 nm/min for 10 min; (b) 50 μm×50 μm F = 22 nm/min for 18 min; (c) 50 μm×50 μm F = 16 nm/min for 25 min.

On SiO_2 surface, the seahorse-like patterns show almost the same characters as on amorphous carbon thin film (Figs. 2(d), 4(a) and (5)). The pattern has an "S" or reverse-"S" backbone measuring 7∼13 μm in length. There are some finlike extrusions pointing away from the backbone, each of which has a triangular shape with a sharp end. As we can see in large scale images (Fig. (5)), the "S" and reverse-"S" chiralities occur with roughly equal probabilities. Besides seahorse patterns, we also find some abnormities, like half seahorse-like patterns and double-head or double-tail patterns; this may be due to inefficient local growth conditions. Seahorse-like patterns on the mica surface also show two chiralities with same probabilities. They also have backbone and finlike extrusions. Unlike the patterns on SiO_2, those finlike extrusions are actually stacks of hexagonal building blocks which can be clearly seen at the end of the extrusions.

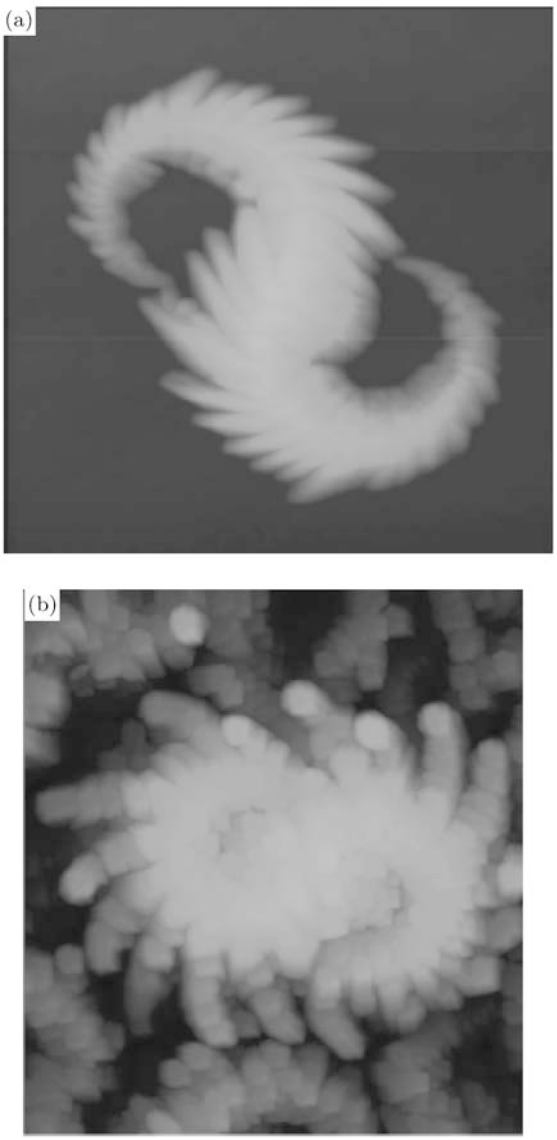


Fig. 4. Typical seahorse-like fractal patterns at different values of deposition flux F: (a) 12 μm×12 μm with substrate of SiO_2; (b) 12 μm×12 μm with substrate of mica.

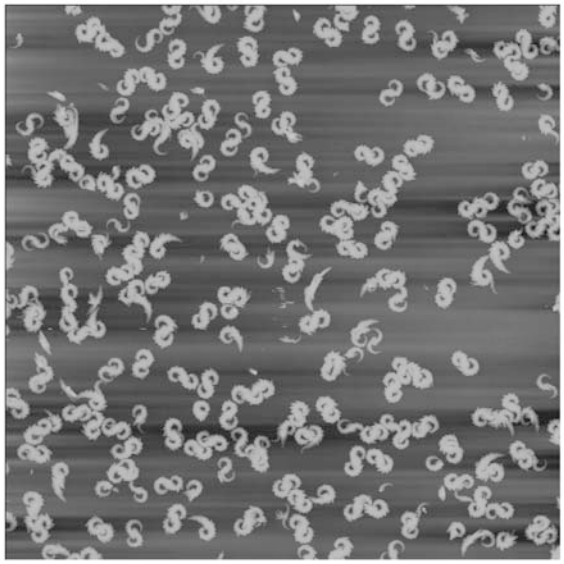


Fig. 5. Large-scale seahorse-like fractal pattern: 100 μm×100 μm, substrate: SiO_2.

The formation of the unique seahorse-like patterns on different surfaces implies that the interactions between TCNQ molecules play an important role in the process. In addition, the interactions between TCNQ and the substrate also affect the growth conditions and some minor features of the pattern.

4. Model and simulations

TEM micro beam diffraction indicates that the TCNQ fractal patterns are composed of many small crystal blocks, and this is in accordance with its topographic images. Two other noteworthy characteristics of the seahorse pattern growth process are that the end of the finlike extrusions and the end of the backbone both have a priority in growth, and that the backbone of the pattern is curved.

Based on these facts, we propose a simple "two-branch" model to simulate the growing process (Fig. 6(a)). The model starts with a branch. Then, two pairs of new branches grow out at both ends of the old branch. We call the original branch the "father branch", the longer new branch the "main branch" (black) which is 1/scale_m of the "father branch" in length, and the shorter new branch the "sub branch" (gray) which is 1/scale_s of the "father branch" in length (scale_s > scale_m). The angles between the "main branch" and the "father branch", and between the "sub-branch" and the "father branch" are angle_mm and angle_ms respectively. In the following step, every new branch becomes a "father branch", and a new branch pair grows out at every end satisfying the length and the angle relations with the new "father branch". By choosing these parameters properly, we can obtain an "S" or reverse-"S" pattern after specific steps as shown in Fig. 6(b). We further substitute branches with rhombic crystal blocks and obtain the final simulation result (Fig. 6(c)) which is consistent with most of the characteristics of our experimental data.

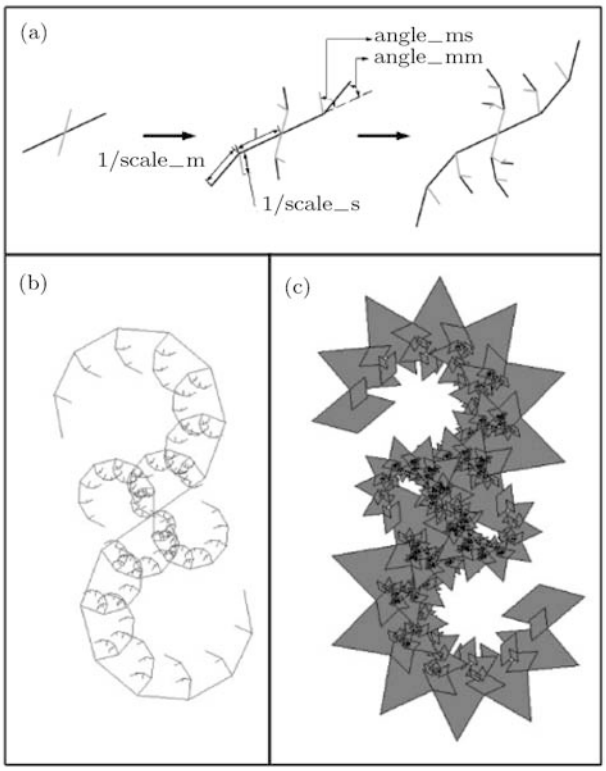


Fig. 6. Seahorse-like pattern simulated by "two-branch" model: (a) First three steps of "two-branch" model; the black branches are longer "main branches" and the gray branches are shorter "sub-branches" in each step; (b) The "S" shape framework is formed after eight steps of "two-branch" growth; (c) Seahorse-like pattern is achieved by further replacing branches with rhombic crystal blocks.

Although this phenomenal model mimics the actual formation of TCNQ seahorse-like patterns, the atomic growth process remains unknown and needs further investigating. In the earlier work about DDAN thin film growth,[27,28] Cai *et al.* claimed that due to the interaction of in-plane electric dipole moment among DDAN molecules, they formed desert-like and forest-like patterns under different growth conditions. But in our system, there is observed no in-plane electric dipole moment of TCNQ molecules, so we need to consider other forms of molecular interaction or even the interactions between crystallites of TCNQ molecules.

5. Summary

We obtained different deposit patterns of TCNQ molecules, including dot patterns, bug-like patterns, seahorse-like patterns and thin films, on SiO_2 surfaces by means of secondary physical vapour deposition. AFM characterizations reveal the interplay between evaporation conditions, molecule–molecule interactions and molecule–substrate interactions in the growth process. A comparison between the seahorse-like patterns on SiO_2 and mica surfaces allows us to reach a good preliminary understanding of the driving force behind this unique fractal pattern. Finally, we proposed a simple model to simulate the growth process of the seahorse-like pattern.

References

[1] Böhringer M, Morgenstem K, Schneider W D, Berndt R, Mauri F, De Vita A and Car R 1999 *Phys. Rev. Lett.* **83** 324

[2] Rosei F, Schunack M, Jiang P, Gourdon A, Lægsgaard E, Stensgaard I, Joachim C and Besenbacher F 2002 *Science* **296** 328

[3] Theobald J A, Oxtoby N S, Phillips M A, Champness N R and Beton P H 2003 *Nature* **424** 1029

[4] Gao H J, Sohlberg K, Xue Z Q, Chen H Y, Hou S M, Ma L P, Fang X W, Pang S J and Pennycook S J 2000 *Phys. Rev. Lett.* **84** 1780

[5] Gao H J and Gao L 2010 *Prog. Surf. Sci.* **85** 28

[6] Zhang Z Y and Lagally M G 1997 *Science* **276** 377

[7] Heringdorf F J M Z, Reuter M C and Tromp R M 2001 *Nature* **412** 517

[8] Verlaak S, Steudel S, Heremans P, Janssen D and Deleuze M S 2003 *Phys. Rev.* B **68** 195409

[9] Kelley T W, Baude P F, Gerlach C, Ender D E, Muyres D, Haase M A, Vogel D E and Theiss S D 2004 *Chem. Mater.* **16** 4413

[10] Cao G Y, Fang F, Ye C N, Xing X Y, Xu H H, Sun D L and Chen G R 2005 *Micron* **36** 285

[11] Brechignac C, Cahuzac P, Carlier F, Colliex C, Leroux J, Masson A, Yoon B and Landman U 2002 *Phys. Rev. Lett.* **88** 196103

[12] Buzio R, Boragno C, Biscarini F, De Mongeot F B and Valbusa U 2003 *Nature Materials* **2** 233

[13] Pedersen J S and Carneiro K 1987 *Rep. Prog. Phys.* **50** 995

[14] Mondio G, Neri F, Gurro G, Patane S and Compagnini G 1996 *J. Mater. Res.* **8** 2627

[15] Ferraris J, Cowan D O, Walatka V and Perlstein J H 1973 *J. Am. Chem. Soc.* **95** 948

[16] Ueda K, Sugimoto T, Endo S, Toyota N, Kohama M, Yamamoto K, Suenaga Y, Morimoto H, Yamaguchi T, Munakata M, Hosoito N, Kanehisa N, Shibamoto Y and Kai Y 1996 *Chem. Phys. Lett.* **261** 295

[17] Gao H J, Xue Z Q and Wu Q D 1994 *Chin. Phys. Lett.* **11** 766

[18] Gao H J, Xue Z Q and Pang S J 1996 *J. Phys.* D **29** 1868

[19] Figgis B N, Sobolev A N, Kepert C J and Kurmoo M 2001 *Acta Crystallogr.* C **57** 991

[20] Vickers E B, Giles I D and Miller J S 2005 *Chem. Mater.* **17** 1667

[21] Ho K C and Liao J Y 2003 *Sensor Actuat. B-Chem.* **93** 370

[22] Gao H J, Xue Z Q, Wu Q D and Pang S J 1994 *J. Mater. Res.* **9** 2216

[23] Gao H J, Xue Z Q, Wu Q D and Pang S J 1996 *Solid State Commun.* **97** 579

[24] Gao H J, Canright G S, Pang S J, Sandler I M, Xue Z Q and Zhang Z Y 1998 *Fractals* **6** 337

[25] Sandler I M, Canright G S, Zhang Z Y, Gao H J, Xue Z Q and Pang S J 1998 *Phys. Lett.* A **245** 233

[26] Sandler I M, Canright G S, Gao H J, Pang S J, Xue Z Q and Zhang Z Y 1998 *Phys. Rev.* E **58** 6015

[27] Cai J M, Bao L H, Guo W, Cai L, Huan Q, Lian J C, Guo H M, Wang K Z, Shi D X, Pang S J and Gao H J 2007 *Chin. Phys. Lett.* **24** 2918

[28] Cai J M, Zhang Y Y, Hu H, Bao L H, Pan L D, Tang W, Li G, Du S X, Shen J and Gao H J 2010 *Chin. Phys.* B **19** 067101

[29] Qian C J, Li H, Zhong R, Luo M B and Ye G X 2009 *Chin. Phys.* B **18** 1947

[30] Su Y F, Li P X, Chen P, Xu Z F and Zhang X L 2009 *Acta Phys. Sin.* **58** 4531 (in Chinese)

[31] Coe S, Woo W K, Bawendi M and Bulovic V 2002 *Nature* **420** 800

[32] Kobayashi S, Nishikawa T, Takenobu T, Mori S, Shimoda T, Mitani T, Shimotani H, Yoshimoto N, Ogawa S and Iwasa Y 2004 *Nature Materials* **3** 317

[33] Street S C, Xu C and Goodman D W 1997 *Ann. Rev. Phys. Chem.* **48** 43

[34] Hartman H, Sposito G and Yang A 1990 *Clays and Clay Minerals* **38** 337